DOI:
10.1016/j.neuron.2012.08.040

Document Version
Publisher's PDF, also known as Version of record

Neuron
Report

Parametric Functional Maps of Visual Inputs to the Tectum

Nikolas Nikolaou,[1,2] Andrew S. Lowe,[1,2] Alison S. Walker,[1] Fatima Abbas,[1] Paul R. Hunter,[1] Ian D. Thompson,[1] and Martin P. Meyer[1,*]
[1]MRC Centre for Developmental Neurobiology, King's College London, Guy's Hospital Campus, London SE1 1UL, UK
[2]These authors contributed equally to this work
*Correspondence: martin.meyer@kcl.ac.uk
http://dx.doi.org/10.1016/j.neuron.2012.08.040

SUMMARY

How features of the visual scene are encoded in the population activity of retinal ganglion cells (RGCs) targeting specific regions of the brain is not well understood. To address this, we have used a genetically encoded reporter of presynaptic function (SyGCaMP3) to record visually evoked activity in the population of RGC axons innervating the zebrafish tectum. Using unbiased voxel-wise analysis of SyGCaMP3 signals, we identify three subtypes of direction-selective and two subtypes of orientation-selective retinal input. Composite parametric functional maps generated across many larvae show laminar segregation of direction- and orientation-selective responses and unexpected retinotopic biases in the distribution of functional subtypes. These findings provide a systematic description of the form, organization, and dimensionality of visual inputs to the brain and will serve as a platform for understanding emergent properties in tectal circuits associated with visually driven behavior.

INTRODUCTION

A central objective of systems neuroscience is to understand how sensory information is encoded at successive levels of the nervous system to generate behavioral output. Classically, this question has been approached at the single neuron level: how do individual neurons at various stages in the sensory-motor pathway process and filter sensory information? But, inevitably, this approach cannot address the relative contribution of individual neurons to the population encoding of sensory information. Recent developments in brain imaging have enabled the emphasis to shift toward population encoding. However, these studies have focused almost exclusively on postsynaptic processing of sensory input. Very little is known on a population basis of the functional input delivered by sensory neurons to a given CNS target. The exception to this rule is the olfactory bulb, where defining the response properties of many glomeruli simultaneously at the sensory input level has provided direct insight into spatiotemporal coding of odorant stimuli (Friedrich and Korsching, 1997; Soucy et al., 2009). Here we provide the first systematic description of the form, organization, and dimensionality of the population of visual inputs to the brain using the optic tectum of larval zebrafish as a model.

At 6 days postfertilization, zebrafish larvae are translucent and exhibit a repertoire of complex visually guided behaviors, making them an excellent model system for imaging studies of visuomotor transformations (Portugues and Engert, 2009). At this stage of development, the larval brain is also small in terms of physical size and number of neurons, allowing activity patterns across a substantial fraction of neurons in the brain to be imaged in a single field of view using optical approaches (Niell and Smith, 2005; Sumbre et al., 2008). The optic tectum, which is used to guide behaviors such as prey capture and predator and obstacle avoidance (Gahtan et al., 2005), has four distinct retinorecipient laminae, and as a rule, the axon of a single retinal ganglion cell (RGC) is restricted to a single lamina (Xiao and Baier, 2007). To examine the nature of the visual input to the tectum, we fused the genetically encoded calcium sensor GCaMP3 to the synaptic vesicle protein synaptophysin (Tian et al., 2009) and generated a stable transgenic line of zebrafish that expresses the resulting probe (SyGCaMP3) specifically in RGCs. This allows us to record visually evoked calcium transients in presynaptic terminals of RGC axons in the intact zebrafish brain. The same strategy has been adopted previously using a synaptophysin-GCaMP2 fusion to study population activity of bipolar cells in the zebrafish retina (Dreosti et al., 2009; Odermatt et al., 2012).

Furthermore, we developed an unbiased voxel-wise analysis strategy that permits functional characterization of the retinal input independent of RGC axon or tectal neuropil morphology and at a spatial scale below that of a presynaptic bouton. This not only allows visual selectivity to be determined on a voxel-by-voxel basis, but also describes visual input to the tectum on a population basis. We have used these techniques to characterize responses to drifting bars. We have identified three subtypes of direction-selective input and two subtypes of orientation-selective inputs. By generating functional parametric maps in individual fish, we find that stratum fibrosum et griseum superficiale (SFGS), which contains the majority of RGC axons that target the tectum, is subdivided into laminae containing either direction- or orientation-selective inputs. Composite parametric maps, generated from multiple larvae, demonstrate that the architecture seen in single animals generalizes to the population while revealing unexpected

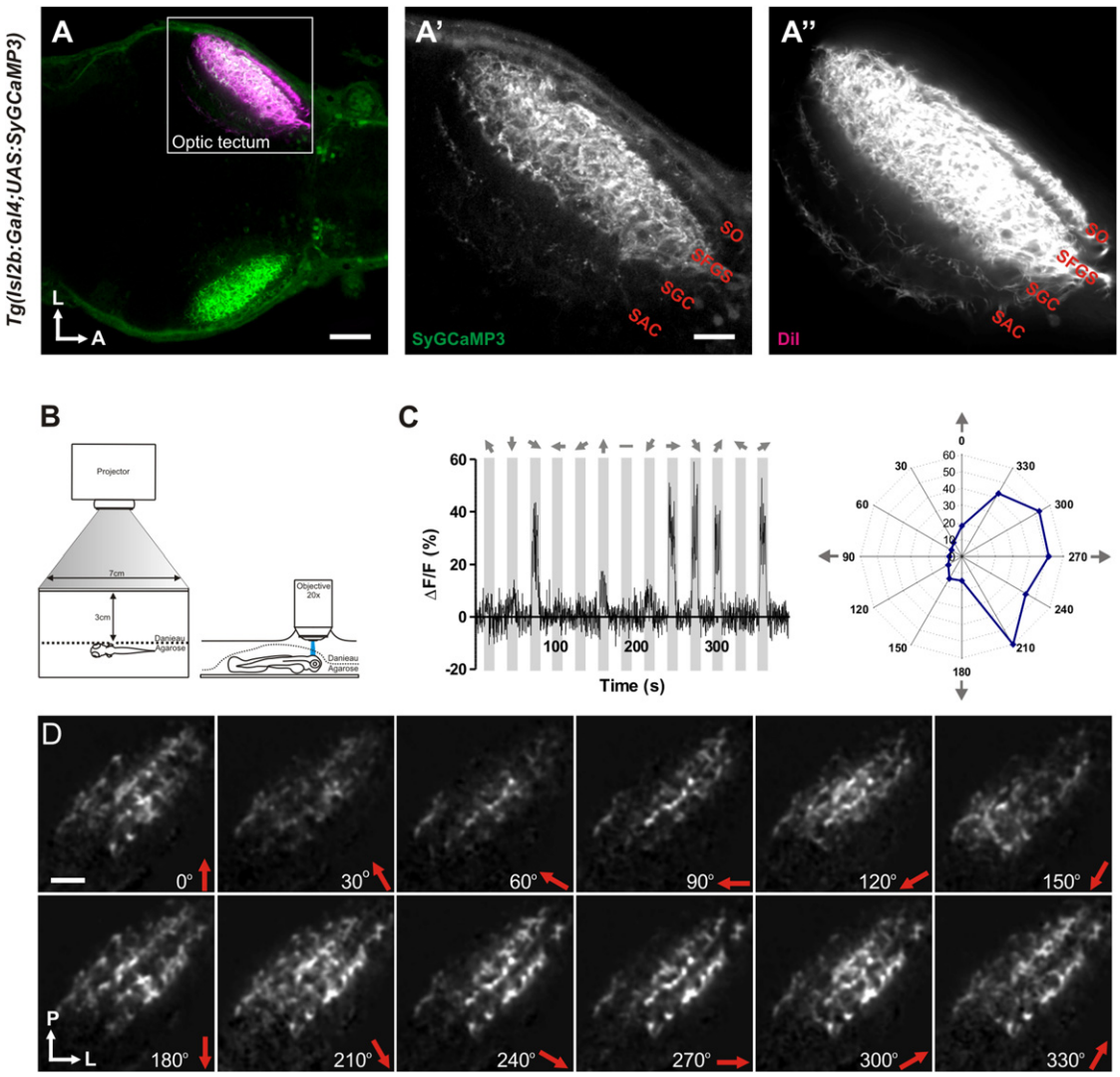

Figure 1. SyGCaMP3 Transgenic Zebrafish and Experimental Set-Up

(A–A″) Dorsal view of a 7 dpf double transgenic Tg(*Isl2b:Gal4;UAS:SyGCaMP3*) zebrafish larva showing SyGCaMP3 expression in RGC axons within the tectal neuropil. DiI, injected into the right eye, labels RGC axons throughout all retinorecipient laminae in the left tectal hemisphere. Boxed region is magnified in (A′) and (A″) (SO, stratum opticum; SFGS, stratum fibrosum et griseum superficiale; SGC, stratum griseum centrale; SAC, stratum album centrale) (L, lateral; A, anterior). (B) Larvae were immobilized in agarose and placed with one eye facing a projection screen. Visually evoked SyGCaMP3 responses were recorded in the contralateral tectum. (C) Representative percentage ΔF/F of a single voxel during a tuning experiment. Stimulus epochs are shown in gray and direction of motion is indicated by arrows. Integral responses in polar plot form are shown to the right. (D) Montage showing integral responses (grayscale) of all voxels (RGC axons) in the tectum. Direction of motion is shown on the bottom right in each panel. Orientation of the image is shown on the bottom left (P, posterior; L, lateral). Scale bars represent 50 μm in (A), 20 μm in (A′), and 20 μm in (D).

retinotopic biases in the distribution of direction- and orientation-selective responses.

RESULTS

Generation of SyGCaMP3 Transgenic Zebrafish

In order to image visually evoked activity in zebrafish RGC axon terminals in vivo, we fused the coding region for zebrafish synaptophysin to the genetically encoded calcium sensor GCaMP3 (Tian et al., 2009) to generate SyGCaMP3 (see Figure S1 available online for probe characterization). To drive expression of SyGCaMP3 in RGCs, we used Tol2-mediated transgenesis (Urasaki et al., 2006) to generate a stable transgenic line of zebrafish that places SyGCaMP3 expression under the control of upstream activator sequences (UASs)—the binding site of the transcriptional activator, GAL4. Crossing the *UAS:SyGCaMP3* transgenic line with the *Isl2b:GAL4* line (Ben Fredj et al., 2010) drives expression in RGC axons throughout all four retinorecipient layers of the tectum in all double transgenic *Isl2b:Gal4;UAS:SyGCaMP3* larvae (hereafter referred to as SyGCaMP3 larvae) (Figures 1A–1A″).

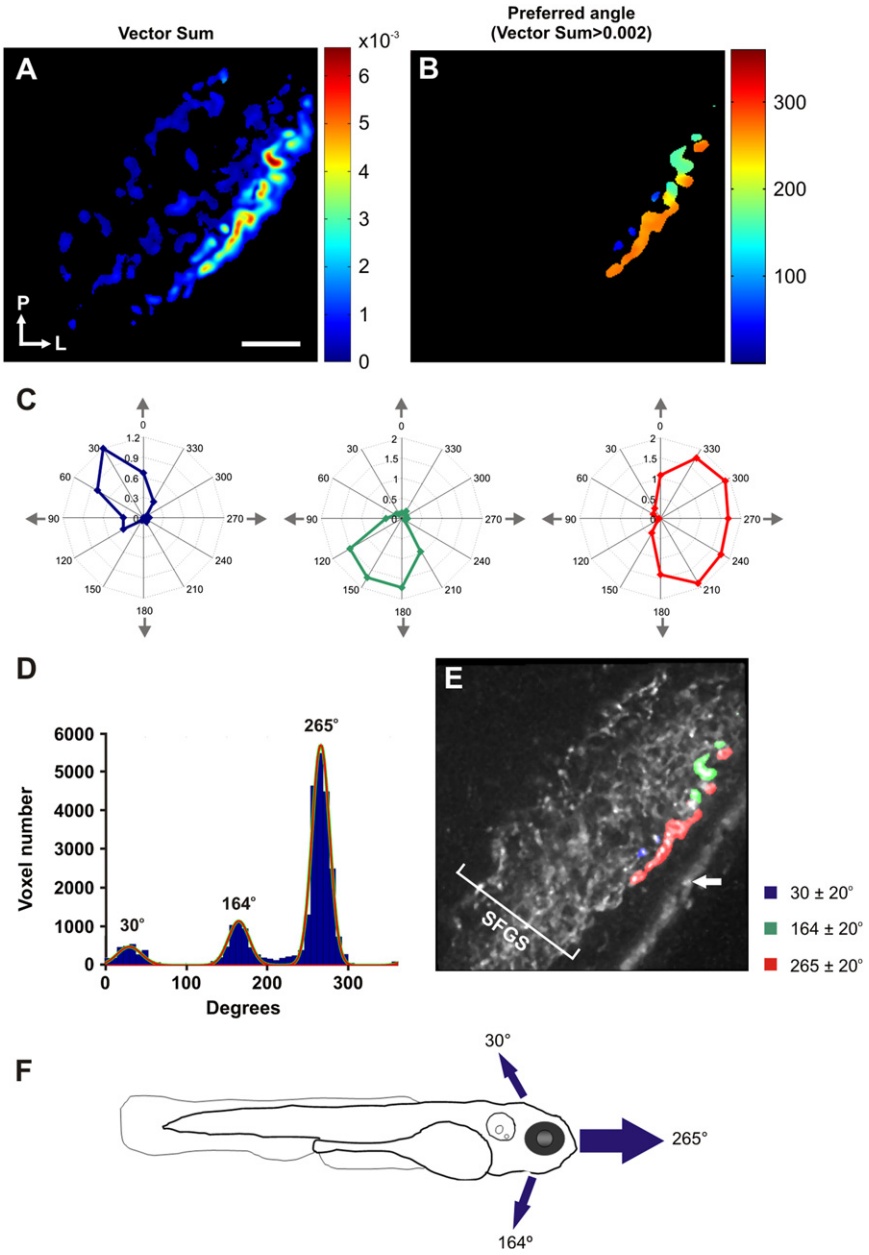

Figure 2. Direction-Selective Responses Are Restricted to a Superficial Layer of SFGS

(A) Voxel-wise vector sum analysis of a single larva. Voxels are color coded according to vector sum (scale shown to the right). (B) A threshold (vector sum > 0.002) applied to the map shown in (A) reveals direction-selective voxels localized to superficial regions of the tectal neuropil. Color coding represents the preferred angle. (C) Polar plots of representative voxels with highly direction-selective responses (color coding as in B). (D) Distribution of vector angles for all direction-selective voxels (23 optical sections from 9 larvae). Fitted von-Mises distributions confirm three populations of direction-selective voxels centered at 30°, 164°, and 265°. (E) Parametric map of a single larva illustrating the three populations of direction-selective responses superimposed onto the mean fluorescence image of SyGCaMP3-expressing axons. Direction-selective responses occur in a superficial layer of SFGS. White arrow indicates skin autofluorescence. (F) Preferred angles of direction-selective responses relative to the larval body axis. Arrows are scaled to reflect the relative proportion of voxels in each population. Scale bar represents 20 μm in (A), as well as in (B) and (E).

In Vivo Imaging and Voxel-Wise Analysis of SyGCaMP3 Signals

We examined visually evoked calcium responses in RGC terminals by presenting light or dark drifting bars (see Supplemental Experimental Procedures), moving in 12 directions to one eye while performing confocal imaging of the contralateral tectum (Figure 1B). To enable fine-scale characterization of retinal inputs, we developed a voxel-wise analysis strategy that is independent of cellular and neuropil morphology. Calculating the integral response over each stimulus epoch enabled tuning curves to be generated for each voxel at a spatial scale below that of an average presynaptic bouton in zebrafish RGCs (Meyer and Smith, 2006 and see Supplemental Experimental Procedures). This approach revealed a complex pattern of responses to visual stimulation and their spatial distributions within the RGC population targeting the tectum (Figures 1C and 1D and Movies S1 and S2).

From such observations two obvious questions emerge: (1) does the voxel-based analysis reveal functional subtypes of retinal input and, if so, (2) what is the functional architecture of this input? To resolve these questions, we parameterized functional responses in the population of retinotectal inputs as direction- or orientation-selective on a voxel-by-voxel basis. To examine direction and orientation selectivity, we used simple, mutually exclusive descriptive statistics: normalized summed vector and 1 − circular variance, respectively, with the complex angle providing the preferred angle for orientation-selective voxels. Direction- and orientation-selective indices (DSIs and OSIs) based on fitted von-Mises distributions were also calculated (Figures S2 and S3).

Direction-Selective Inputs Target the Superficial Layers of SFGS

Voxel-wise vector sum analysis quantified the extent and position of direction-selective responses in the tectum of individual larvae (Figure 2A). An empirically derived magnitude threshold was used to examine both the tectal location and angle of direction-selective voxels. Strikingly, this shows a very restricted

distribution both in preferred directions and localization within the tectal neuropil of all single subjects analyzed. This is illustrated in Figure 2B, where voxels are color coded according to summed vector angle. For each voxel, a tuning curve can be derived (examples shown in Figure 2C) and the resultant angles cumulated across the population of all imaged larvae (Figure 2D). These cumulative data reveal distinct distributions in the direction selectivity of retinotectal inputs. Iteratively fitting three summed von-Mises distributions to the population histogram reveal nonoverlapping populations with peaks centered at 30°, 164°, and 265° with the dominant input corresponding to tail-to-head motion (relative areas under the fitted von-Mises curves being 0.09, 0.17, and 0.74, respectively). Figure 2F shows these angles relative to the larval body axis.

A parametric map of direction selectivity in each subject representing the three populations of responses centered on the fitted von-Mises distributions ±20° was generated and superimposed onto the mean fluorescence image of SyGCaMP3-expressing axons in the tectal neuropil. An illustrative map shown in Figure 2E shows several striking features; directional voxels cluster according to preferred direction, and these clusters are restricted to a superficial layer of SFGS. The deeper portions of SFGS and the remaining, more sparsely innervated laminae (stratum opticum [SO], stratum griseum centrale [SGC], and stratum album centrale [SAC]) contain few, if any, direction-selective voxels. A further consistent finding is that within the majority of individual larvae, the relative proportions of preferred angles reflect the distributions in cumulative population data. An alternative metric for directionality (DSI) gives very similar response distributions to those found using the normalized summed vector sum (Figure S2). This figure also shows an example of a single RGC labeled with SyGCaMP3 that is selective for tail-to-head motion. This confirms that the voxel-wise approach to analysis of the population data reliably reflects functional cell types. These data identify in zebrafish three distinct functional forms of direction-selective retinotectal input. Furthermore, parametric mapping indicates that, in all individual zebrafish larvae, responses cluster according to subtype within the superficial layers of SFGS.

Orientation-Selective Inputs Are Broadly Distributed within SFGS

In a number of species, including adult goldfish, some RGCs demonstrate orientation selectivity for moving bars (Maximov et al., 2005). To probe for orientation tuning in the retinotectal input, we calculated the 1 − circular variance for each responding voxel (Figure 3A), a metric that reveals symmetric tuning. By applying a conservative threshold of <0.4, we identified voxels that either are strongly orientation selective or have no selectivity (responded to all orientations). Using 1 − circular variance to examine preferred orientation on a voxel-by-voxel basis reveals clustering of voxels according to motion preference as derived from the calculated complex angle (Figure 3B). Polar plots from individual voxels illustrate such highly orientation-selective responses (Figure 3C). Examining the cumulative distribution of complex angles across all larvae imaged reveals two clear populations (Figure 3D) plus a baseline component that reflects the voxels responding to all orientations with noise randomly and evenly distributing the calculated complex angles. Iteratively fitting two summed von-Mises distributions (constrained with bimodal distributions separated by 180° and equal concentration) plus a baseline component to the histogram data derived distinct population peaks centered at 105°/285° and 172°/352° (Figure 3D). These correspond to motion of vertically oriented bars moving along the horizontal axis (horizontally tuned) and horizontally oriented bars moving along the vertical axis (vertically tuned), respectively (Figure 3G). The largest fraction of orientation-selective voxels is tuned to vertical motion. Within all individual larvae examined, the relative proportions of voxels selective for vertical and horizontal motion generally reflect those in cumulative population data.

From the distributions identified in Figure 3D, we generated parametric maps in which voxels are color coded according to orientation preference and superimposed on the fluorescence image of the tectal neuropil (Figures 3E and 3F). These maps, which allow examination of functional architecture in individual larvae, reveal that in all subjects, orientation-selective inputs are broadly distributed across SFGS and that voxels tend to cluster according to orientation preference. What is evident from the two examples of separate larvae is that within the orientation-selective domain, the organization of the two subtypes can be variable across subjects. The same orientation-selective inputs, with similar tectal distributions, were identified using the OSI metric (Figure S3). This figure also shows examples of single orientation-selective RGCs expressing SyGCaMP3 that are selective for either horizontal or vertical motion.

Composite Parametric Maps Reveal Retinotopic Biases of Functional Subtypes

The functional parametric maps of individual larvae shown in Figures 2 and 3 suggest regional differences in the distribution of direction- and orientation-selective inputs to the zebrafish tectum. To examine in more detail the spatial organization of direction- and orientation-selective responses in SFGS, we spatially coregistered data from all larvae to create single composite maps for each parameter (see Supplemental Experimental Procedures). The large panels in Figures 4A and 4B show color-coded composite parametric maps for the three direction-selective subtypes and the two orientation-selective subtypes. The minor panels illustrate the separate composite parametric maps of each subtype, together with histograms illustrating the ranges of responses used to generate each composite. In each parametric map, voxel brightness is proportional to the summed incidence of each functional subtype across all larvae. In Figures 4C and 4D, the combined composites are rotated and used to derive line plots of the summed incidence of each functional subtype across two axes that represent the laminar (x axis) and topographic (y axis) organization of the tectal neuropil. The composite analysis allows us to be much more confident about the functional architecture of visual input to the tectum compared to descriptions of individual confocal sections. For example, while direction-selective input is almost entirely confined to a superficial layer within SFGS (as seen in individual sections), there is also a minor input to deeper SFGS (Figure 4C) that was not considered a robust finding at the level of single sections. Furthermore, the sublaminar relationship of

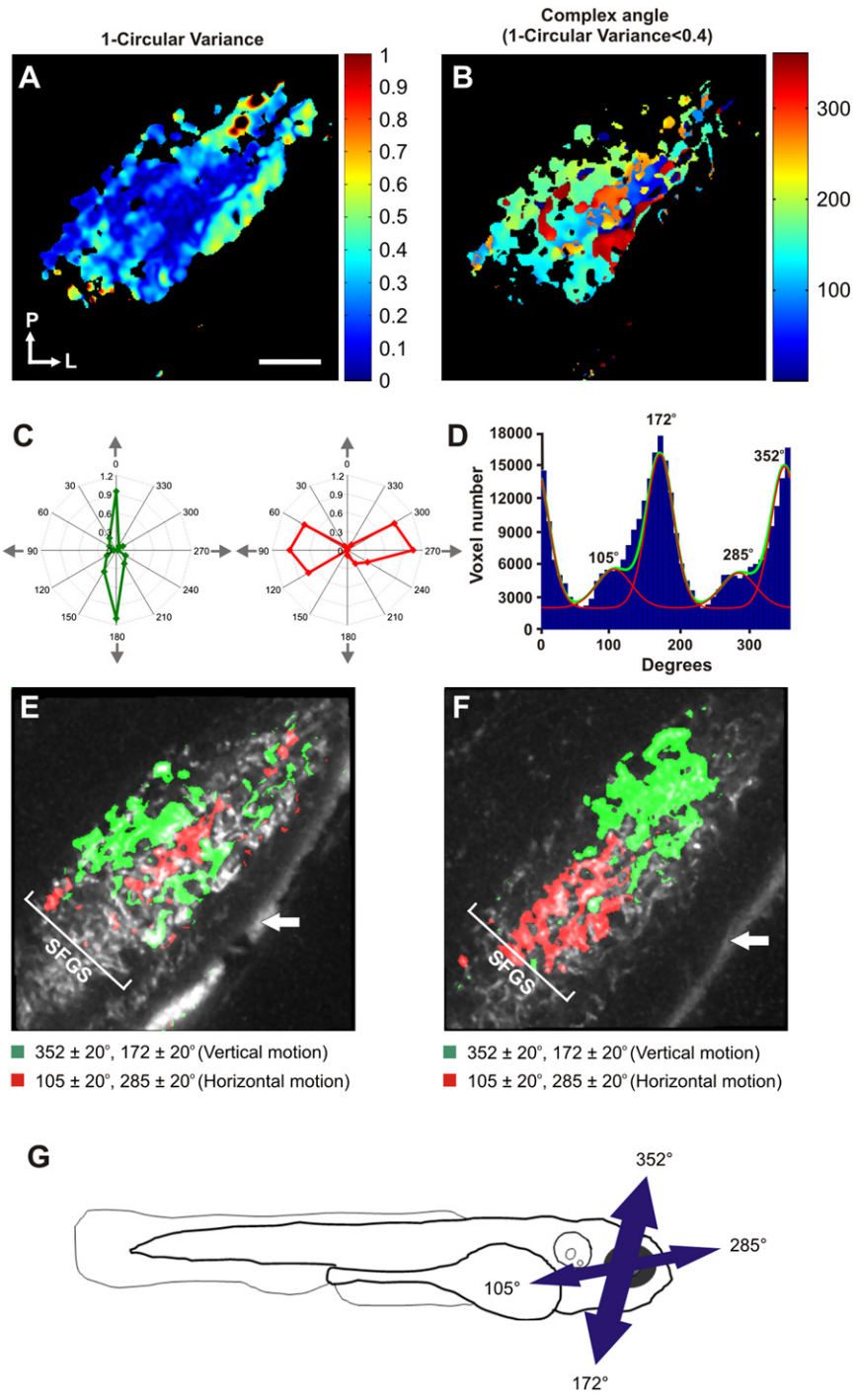

Figure 3. Orientation-Selective Responses Are Broadly Distributed throughout SFGS

(A) Voxel-wise analysis of 1 − circular variance from a single larva. Voxels are color coded according to 1 − circular variance (scale to the right). (B) A threshold (1 − circular variance < 0.4) applied to the map shown in (A) reveals orientation-selective voxels. Color coding represents the complex angle. (C) Polar plots showing highly orientation-selective responses in individual voxels (color coding as in B). (D) Distribution of complex angles of all orientation-selective voxels. (Data are from 23 different optical sections from 9 larvae.) Fitted bimodal von-Mises distributions reveal two populations of orientation-selective response centered at 352°(+180°) and 105°(+180°) (relative fractions of the total are 0.54 and 0.17, respectively). The baseline population represents the nontuned population of voxels responding approximately equally to all orientations (0.28). (E and F) Parametric maps of two larvae illustrating the spatial arrangement of the two populations of orientation-selective responses in the deeper portion of SFGS. White arrow indicates skin autofluorescence. (G) Preferred angles of orientation-selective responses relative to the larval body axis. Arrows are scaled to reflect relative proportion of voxels in each population. Scale bar represents 20 μm in (A), as well as in (B), (E), and (F).

direction- and orientation-selective voxels are compared directly in the relative plot shown in Figure 4E, which confirms the segregation of direction- and orientation-selective responses in the tectal neuropil. The area of intersection (shaded) between all direction-selective (solid lines) and orientation-selective (dashed lines) voxels was only 14% of the total area.

The surprising finding from the composite analysis is that both direction- and orientation-selective inputs cluster with topographic biases. All directional inputs are confined to the posterior half of the tectum, and within this domain, the inputs centered on 30° and those centered on 164° are confined to the anterior and posterior portions, respectively. The orientation-selective composite also reveals retinotopic differences in the distribution of horizontally and vertically tuned inputs (Figure 4D). Vertically orientated inputs are distributed throughout SFGS but are more concentrated in the posterior tectum, while horizontally tuned voxels are concentrated at the anterior pole. Very similar composites were obtained using OSI and DSI measures of orientation and direction tuning (Figure S4). The composite maps thus allow more robust and surprising conclusions to be made about the functional architecture of direction- and orientation-selective visual input into the zebrafish tectum.

DISCUSSION

Understanding how visual sensory information is processed within the brain requires a description of the form and organization of all inputs to retinorecipient structures. We have provided

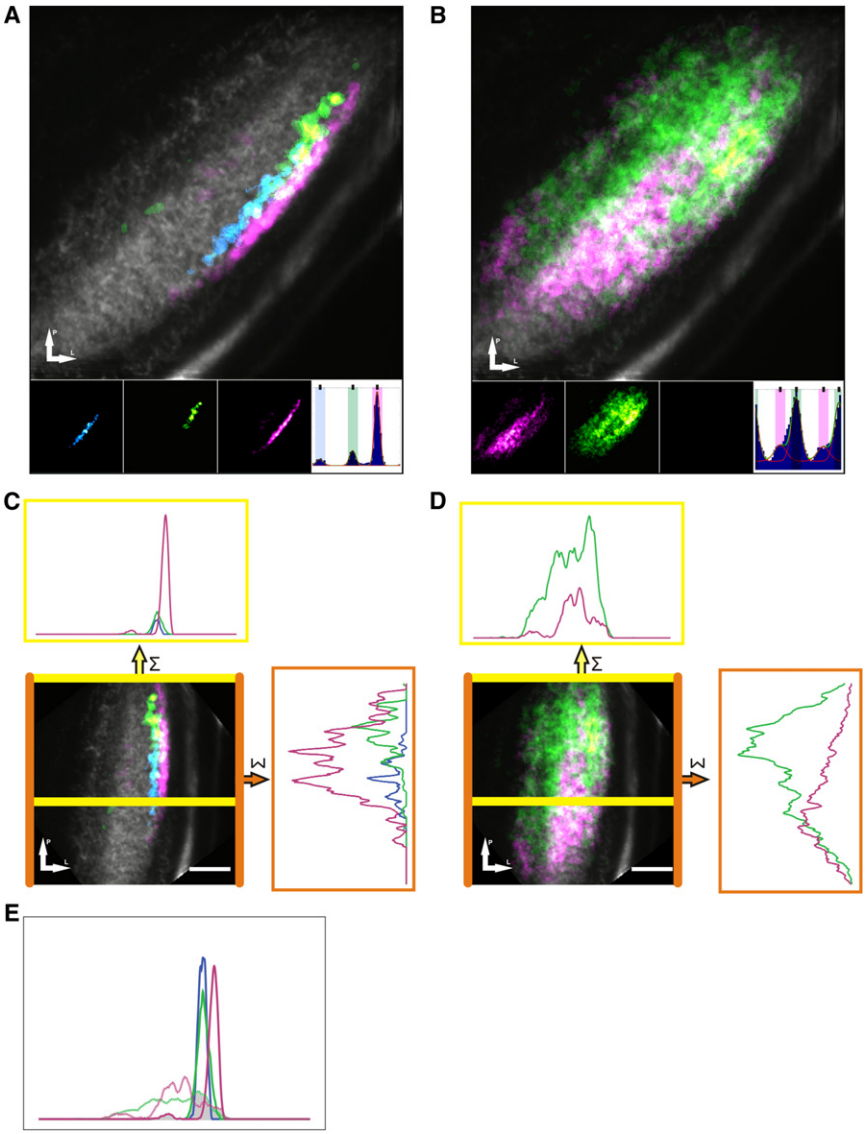

Figure 4. Composite Maps Reveal a Laminar and Retinotopic Organization of Direction- and Orientation-Selective Responses

(A and B) Combined composite parametric maps that represent the spatial organization of responses across all subjects color coded for individual subpopulations of direction-selective (A) and orientation-selective (B) responses overlaid on an anatomical image (grayscale). Voxels that lie within ±20° of the peak of each fitted von-Mises distribution (inset histograms) are color coded and mapped on the individual (inset) and combined composite maps. (C and D) The composite maps of direction-selective (C) and orientation-selective (D) responses, respectively, are rotated to enable line plots representing the summed incidence across each axis: the area between the yellow lines represents an approximately linear segment of the neuropil to assess lamination and the area between the orange lines represents visual field to assess retinotopic organization. (E) Relative histograms of direction-selective responses and orientation-selective responses across laminar of the tectal neuropil (derived from lower line plots in C and D). Note that the area of intersection between all direction-selective (solid lines) and orientation-selective (dashed lines) voxels was only 14% of the total area—confirming the laminar segregation of direction- and orientation-selective responses. Scale bar represents 20 μm in (C) and (D).

a partial description for the optic tectum by generating transgenic zebrafish that express a presynaptically targeted, genetically encoded calcium sensor (SyGCaMP3) in RGCs. This allows functional imaging of the population of visual inputs to the tectum specifically that, when combined with the voxel-wise analysis approach, allows us to characterize the stimulus selectivity of retinal input to the tectum. We have defined five distinct classes of response to drifting bars: three subtypes of direction selective and two subtypes of orientation selective. The number of zebrafish direction-selective retinal subtypes and their preferred directions of motion match those identified in electrophysiological studies of adult goldfish (Maximov et al., 2005) and also those of the on-direction-selective ganglion cells (On-DSGCs) that project to the nuclei of the accessory optic system (AOS) in mammals (Yonehara et al., 2009). Our data therefore suggest that, like the AOS of mammals, the zebrafish tectum may play a role in stabilizing the retinal image during self-motion. Indeed, tectal ablations in zebrafish have been shown to alter, although not eliminate, the optokinetic response by reducing the frequency of saccades (Roeser and Baier, 2003). Our population analysis of direction-selective cells in zebrafish extends the goldfish studies by providing an estimate of the relative proportions of each response subtype targeting the tectum: responses to bars moving in the tail-to-head direction (265°) dominate the direction-selective input, while responses to horizontal bars moving along the vertical axis dominate the orientation-selective input.

Importantly, by generating parametric response maps, we were also able to examine in detail the spatial distribution of all subtypes within the tectal neuropil. This shows clear laminar segregation in the distribution of direction- and orientation-selective inputs within SFGS of the tectal neuropil. Superficially this may not seem surprising given that individual RGC axons terminate within single laminae in the zebrafish tectum (Xiao and Baier, 2007; Xiao et al., 2011)—a conclusion echoed in morphological studies of the mammalian superior colliculus (Huberman et al., 2009; Kay et al., 2011; Kim et al., 2010). However, we find that the three direction-selective subtypes terminate in only two discrete layers within the most superficial portion of SFGS. Such tight laminar organization is not found for orientation-selective input, which is found throughout SFGS with no

clear laminar segregation between subtypes. Does this suggest multiple classes of orientation-selective RGCs? Multiple subclasses have recently been demonstrated in a previously reported single functional class of ON-OFF direction-selective RGC tuned to posterior motion. The subclasses differ in their physiology, morphology, and, most pertinently, in the pattern of their axonal projections to the superior colliculus (Rivlin-Etzion et al., 2011). The composite parametric maps we have generated also reveal biases within direction- and orientation-selective domains. Orientation-selective inputs tuned to bars moving along the vertical and horizontal axes are concentrated in posterior and anterior tectum, respectively. But most striking is the restriction of direction-selective responses to the posterior half of the tectum and the stereotyped differences in stimulus selectivity within this domain. There are rare accounts of ganglion cells being confined to retinal segments. For example, somatostatin-positive alpha cells in cat and rabbit retina are largely restricted to inferior retina (Sagar, 1987; White and Chalupa, 1991) and in the mouse, a subset of RGCs selective for upward motion occurs in dorsal retina (Kay et al., 2011). Because our approach is a functional characterization at the voxel level, retinotopic variations need not necessarily reflect regional variations in the distribution of different morphological classes of RGC. For example, there may be regional differences in the circuits driving RGC activity within the retina. Such differences, which have been reported in the distributions of neurotransmitter and neuromodulator systems with various classes of retinal neurons (Wilson et al., 2011), could influence the function of a cell in a given morphological class. Presynaptic calcium levels may also be modulated by inputs onto RGC terminals within the tectum itself (Edwards and Cline, 1999). An obvious question is whether the functional retinotopic biases in RGC input is reflected in the postsynaptic tectal neurons. The rostro-caudal dendritic extent for at least three tectal cell types is well below the size of the RGC functional domains that we have identified (Robles et al., 2011). Such spatially restricted sampling of RGCs by tectal neurons suggests that the regional biases in direction and orientation selectivity could be preserved in the population of postsynaptic tectal neurons. Indeed, a previous functional imaging study has suggested that retinotopic biases in direction-selective responses do indeed exist in the population of tectal cells in the zebrafish tectum (Niell and Smith, 2005). While the underlying reasons for it are unknown, the functional architecture we have described may reflect an evolutionary solution that minimizes wiring costs associated with integrating and processing visual stimuli that are perhaps ethologically related (Chklovskii and Koulakov, 2004).

Our description of the diversity and organization of inputs to the tectum will also provide a platform for studying emergence in tectal circuits. The property of emergence in neural networks, whereby a neuron produces an output that is not explicitly present in any of its individual inputs, is not well understood. The principal reason is that while the output of individual cells is simple to quantify, determining information about the input that may arise from tens to hundreds of cells is incredibly difficult. Indeed, recent attempts in the retina (Briggman et al., 2011) and visual cortex (Bock et al., 2011) using serial reconstruction at the nanoscale resolution are revealing the size of the challenge. Both of these studies are searching for rules of connectivity that explain the emergent functional properties of neurons. Our aims are similar in that we wish to understand the form and organization of retinal inputs to the whole tectum—global rather than local functional architecture. That is, rather than dissect the inputs to an individual tectal neuron (bottom up), we have adopted a top-down approach that provides information on the diversity and organization of inputs to the tectum as a whole. By extending this approach to a full characterization of the functional dimensionality of retina, functional inputs together with the relative individual probabilistic spatial organization (maps) will be a powerful resource that will reveal not only the diversity of inputs to all tectal cells but also the relative proportions of synaptic input to any single postsynaptic tectal cell. Further, knowing the inputs to the whole tectum will reveal whether the output of an individual tectal cell has any emergent properties. Such approaches will form the basis for understanding how circuits in the tectum translate sensory stimuli into behavior, a fundamental goal in systems neuroscience.

EXPERIMENTAL PROCEDURES

Please see Supplemental Experimental Procedures for details.

SUPPLEMENTAL INFORMATION

Supplemental Information includes four figures, Supplemental Experimental Procedures, and three movies and can be found with this article online at http://dx.doi.org/10.1016/j.neuron.2012.08.040.

ACKNOWLEDGMENTS

We wish to thank Matt Grubb for comments on the manuscript, Koichi Kawakami for Tol2 reagents, and Juan Burrone for hippocampal cultures. A.S.L. is supported by a Wellcome Trust program grant (083205) awarded to I.D.T., A.S.W is supported by a Medical Research Council (MRC) PhD studentship, N.N., F.A., P.R.H., and M.P.M. are supported by MRC project grants and a Career Development Award awarded to M.P.M. (G0801242, G1100162, and G0600107).

Accepted: August 9, 2012
Published: October 17, 2012

REFERENCES

Ben Fredj, N., Hammond, S., Otsuna, H., Chien, C.B., Burrone, J., and Meyer, M.P. (2010). Synaptic activity and activity-dependent competition regulates axon arbor maturation, growth arrest, and territory in the retinotectal projection. J. Neurosci. *30*, 10939–10951.

Bock, D.D., Lee, W.C., Kerlin, A.M., Andermann, M.L., Hood, G., Wetzel, A.W., Yurgenson, S., Soucy, E.R., Kim, H.S., and Reid, R.C. (2011). Network anatomy and in vivo physiology of visual cortical neurons. Nature *471*, 177–182.

Briggman, K.L., Helmstaedter, M., and Denk, W. (2011). Wiring specificity in the direction-selectivity circuit of the retina. Nature *471*, 183–188.

Chklovskii, D.B., and Koulakov, A.A. (2004). Maps in the brain: what can we learn from them? Annu. Rev. Neurosci. *27*, 369–392.

Dreosti, E., Odermatt, B., Dorostkar, M.M., and Lagnado, L. (2009). A genetically encoded reporter of synaptic activity in vivo. Nat. Methods *6*, 883–889.

Edwards, J.A., and Cline, H.T. (1999). Light-induced calcium influx into retinal axons is regulated by presynaptic nicotinic acetylcholine receptor activity in vivo. J. Neurophysiol. *81*, 895–907.

Friedrich, R.W., and Korsching, S.I. (1997). Combinatorial and chemotopic odorant coding in the zebrafish olfactory bulb visualized by optical imaging. Neuron *18*, 737–752.

Gahtan, E., Tanger, P., and Baier, H. (2005). Visual prey capture in larval zebrafish is controlled by identified reticulospinal neurons downstream of the tectum. J. Neurosci. *25*, 9294–9303.

Huberman, A.D., Wei, W., Elstrott, J., Stafford, B.K., Feller, M.B., and Barres, B.A. (2009). Genetic identification of an On-Off direction-selective retinal ganglion cell subtype reveals a layer-specific subcortical map of posterior motion. Neuron *62*, 327–334.

Kay, J.N., De la Huerta, I., Kim, I.J., Zhang, Y., Yamagata, M., Chu, M.W., Meister, M., and Sanes, J.R. (2011). Retinal ganglion cells with distinct directional preferences differ in molecular identity, structure, and central projections. J. Neurosci. *31*, 7753–7762.

Kim, I.J., Zhang, Y., Meister, M., and Sanes, J.R. (2010). Laminar restriction of retinal ganglion cell dendrites and axons: subtype-specific developmental patterns revealed with transgenic markers. J. Neurosci. *30*, 1452–1462.

Maximov, V., Maximova, E., and Maximov, P. (2005). Direction selectivity in the goldfish tectum revisited. Ann. N Y Acad. Sci. *1048*, 198–205.

Meyer, M.P., and Smith, S.J. (2006). Evidence from in vivo imaging that synaptogenesis guides the growth and branching of axonal arbors by two distinct mechanisms. J. Neurosci. *26*, 3604–3614.

Niell, C.M., and Smith, S.J. (2005). Functional imaging reveals rapid development of visual response properties in the zebrafish tectum. Neuron *45*, 941–951.

Odermatt, B., Nikolaev, A., and Lagnado, L. (2012). Encoding of luminance and contrast by linear and nonlinear synapses in the retina. Neuron *73*, 758–773.

Portugues, R., and Engert, F. (2009). The neural basis of visual behaviors in the larval zebrafish. Curr. Opin. Neurobiol. *19*, 644–647.

Rivlin-Etzion, M., Zhou, K., Wei, W., Elstrott, J., Nguyen, P.L., Barres, B.A., Huberman, A.D., and Feller, M.B. (2011). Transgenic mice reveal unexpected diversity of on-off direction-selective retinal ganglion cell subtypes and brain structures involved in motion processing. J. Neurosci. *31*, 8760–8769.

Robles, E., Smith, S.J., and Baier, H. (2011). Characterization of genetically targeted neuron types in the zebrafish optic tectum. Front Neural Circuits *5*, 1.

Roeser, T., and Baier, H. (2003). Visuomotor behaviors in larval zebrafish after GFP-guided laser ablation of the optic tectum. J. Neurosci. *23*, 3726–3734.

Sagar, S.M. (1987). Somatostatin-like immunoreactive material in the rabbit retina: immunohistochemical staining using monoclonal antibodies. J. Comp. Neurol. *266*, 291–299.

Soucy, E.R., Albeanu, D.F., Fantana, A.L., Murthy, V.N., and Meister, M. (2009). Precision and diversity in an odor map on the olfactory bulb. Nat. Neurosci. *12*, 210–220.

Sumbre, G., Muto, A., Baier, H., and Poo, M.M. (2008). Entrained rhythmic activities of neuronal ensembles as perceptual memory of time interval. Nature *456*, 102–106.

Tian, L., Hires, S.A., Mao, T., Huber, D., Chiappe, M.E., Chalasani, S.H., Petreanu, L., Akerboom, J., McKinney, S.A., Schreiter, E.R., et al. (2009). Imaging neural activity in worms, flies and mice with improved GCaMP calcium indicators. Nat. Methods *6*, 875–881.

Urasaki, A., Morvan, G., and Kawakami, K. (2006). Functional dissection of the Tol2 transposable element identified the minimal cis-sequence and a highly repetitive sequence in the subterminal region essential for transposition. Genetics *174*, 639–649.

White, C.A., and Chalupa, L.M. (1991). Subgroup of alpha ganglion cells in the adult cat retina is immunoreactive for somatostatin. J. Comp. Neurol. *304*, 1–13.

Wilson, M., Nacsa, N., Hart, N.S., Weller, C., and Vaney, D.I. (2011). Regional distribution of nitrergic neurons in the inner retina of the chicken. Vis. Neurosci. *28*, 205–220.

Xiao, T., and Baier, H. (2007). Lamina-specific axonal projections in the zebrafish tectum require the type IV collagen Dragnet. Nat. Neurosci. *10*, 1529–1537.

Xiao, T., Staub, W., Robles, E., Gosse, N.J., Cole, G.J., and Baier, H. (2011). Assembly of lamina-specific neuronal connections by slit bound to type IV collagen. Cell *146*, 164–176.

Yonehara, K., Ishikane, H., Sakuta, H., Shintani, T., Nakamura-Yonehara, K., Kamiji, N.L., Usui, S., and Noda, M. (2009). Identification of retinal ganglion cells and their projections involved in central transmission of information about upward and downward image motion. PLoS ONE *4*, e4320.